

Article

# Unsteady Stagnation-Point Flow and Heat Transfer Over a Permeable Exponential Stretching/Shrinking Sheet in Nanofluid with Slip Velocity Effect: A Stability Analysis

Nor Fadhilah Dzulkifli <sup>1,2,\*</sup>, Norfifah Bachok <sup>2</sup>, Nor Azizah Jacob <sup>1</sup>, Norihan Md Arifin <sup>2</sup> and Haliza Rosali <sup>2</sup>

<sup>1</sup> Department of Mathematics, Faculty of Computer and Mathematics Sciences, Universiti Teknologi MARA Pahang, Bandar Pusat Jengka 26400, Pahang, Malaysia; nor\_azie@yahoo.com

<sup>2</sup> Department of Mathematics and Institute for Mathematical Research, Universiti Putra Malaysia, UPM Serdang 43400, Selangor, Malaysia; norfifah@upm.edu.my (N.B.); norihana@upm.edu.my (N.M.A.); liza\_r@upm.edu.my (H.R.)

\* Correspondence: norfadhilah199@gmail.com; Tel.: +6-01-2960-3932

Received: 26 September 2018; Accepted: 8 October 2018; Published: 06 November 2018



**Abstract:** A model of unsteady stagnation-point flow and heat transfer over a permeable exponential stretching/shrinking sheet with the presence of velocity slip is considered in this paper. The nanofluid model proposed by Tiwari and Das is applied where water with Prandtl number 6.2 has been chosen as the base fluid, while three different nanoparticles are taken into consideration, namely Copper, Alumina, and Titania. The ordinary differential equations are solved using boundary value problem with fourth order accuracy (bvp4c) program in Matlab to find the numerical solutions of the skin friction and heat transfer coefficients for different parameters such as stretching/shrinking, velocity slip, nanoparticle volume fraction, suction/injection, and also different nanoparticles, for which the obtained results (dual solutions) are presented graphically. The velocity and temperature profiles are presented to show that the far field boundary conditions are asymptotically fulfilled, and validate the findings of dual solutions as displayed in the variations of the skin friction and heat transfer coefficients. The last part is to perform the stability analysis to determine a stable and physically-realizable solution.

**Keywords:** stability analysis; stagnation-point flows; exponential stretching/shrinking sheet; nanofluid; velocity slip effect

## 1. Introduction

The stagnation-point flow is a flow that explains the behavior of the fluid motion near the stagnation region. This type of flow happens when the flow hits the solid surface and the fluid velocity at the stagnation-point equals zero. Some applications has been reported where the stagnation-point flow is applied, for instance in dentistry by Yang et al. [1], and air purification as presented by Montecchio et al. [2]. Recently, the study on the flow over an exponential stretching/shrinking sheet has received more attention than for ordinary stretching/shrinking sheets due to its wider applications, as mentioned by Pavithra et al. [3]. Further, Zaib et al. [4] studied the unsteady boundary layer flow and heat transfer passes through an exponential shrinking sheet in a Copper water nanofluid with the presence of a suction effect. The effects of joule heating and thermal radiation on the Magnetohydrodynamics (MHD) boundary layer flow over an exponential stretching sheet in a porous medium immersed in nanofluid was investigated by Rao et al. [5]. Furthermore, Aleng et al. [6] applied

the Buongiorno model to study the flow and heat transfer over an exponential sheet in nanofluid. However, there are only a few works that studied the stagnation-point flow over the exponential sheet, e.g., Bachok et al. [7], who applied the Tiwari and Das model to study the flow and heat transfer over an exponential stretching/shrinking sheet. Bhattacharyya et al. [8] considered the stagnation-point flow as well as the heat transfer passing through an exponential shrinking sheet. Instead of an exponentially shrinking sheet, Rehman et al. [9] in their work studied the MHD stagnation-point flow of a nano-material over an exponentially stretching sheet in a three-dimensional system using the Tiwari and Das model. They considered three types of nanoparticles, namely Copper oxide, Magnetite, and Alumina, whilst water was chosen as the base fluid. Practical applications can be found in industrial processes such as the cooling of extruded materials by inward-directed fan or conical liquid jets, as mentioned by Wong et al. [10].

A new class of heat transfer fluid, namely nanofluid, is introduced by Choi and Eastman [11], due to the low thermal conductivity property demonstrated by the base fluids. This kind of fluid can be obtained by diffusing nanoparticles into base fluids such as water, ethanol glycol, and oil, which increases the surface area for transferring heat. Meanwhile, there are two types of nanofluid models that can be considered in investigations of the behavior of the nanofluid: the Buongiorno [12] and the Tiwari and Das models [13]. The Tiwari and Das model, also known as the “single phase” model, studies the effects of nanoparticle volume fractions for different nanoparticles, whilst the Buongiorno model or “two phase” model focuses on Brownian motion and the thermophoresis effects of the nanoparticles. In addition, a comparison between the single phase and two phase nanofluid models has been undertaken numerically by Akbari et al. [14] for turbulent forced convection; it was found that the results from the single phase model approach the results from experimental findings compared to those obtained from a two phase model for almost conditions. A part from that, the thermal performance of the nanofluid can be affected by considering different types, nanoparticle volume fractions, sizes, as well as diameters of the nanoparticles, as studied by Ebrahimi et al. [15] and Pang et al. [16], who found that nanofluids can be considered an excellent choice for any application which seeks to optimize heat transfer processes. Hence, the emergence of nanofluids was a milestone in heat transfer enhancement, which is required in many fields, for example, energy saving, refrigeration systems, solar collector, and the automotive industry. These examples of nanofluid applications are discussed in numerous papers [17–21]. Many researches have considered nanofluids in their work covering various scopes, surfaces, objects, and also effects, e.g., [22–28]. Pour and Nassab [29] investigated the single-phase laminar convection of nanofluids over a two-dimensional (2D) horizontal backward facing step (BFS) depending numerically on the bleeding condition (suction/injection). In this work, it was found that the skin friction coefficient increased as the suction and volume fraction of the effect of Copper nanoparticles increased.

The stability analysis is introduced by Merkin [30] to investigate the stability of dual solutions which obtained when the mixed convection in a porous medium problem is solved. Merkin considered a time-dependent problem and found that the upper branch (first solution) was a stable solution, while the lower branch (second solution) was not. This pioneering work offered a proper way to determine the stability of every solution that may exist. Many authors have applied stability analyses in their papers when more than one solution was obtained; some examples can be found in these papers, [31–41], which invariably arrived at the same conclusions on the first and second solutions as Merkin [27].

This study is an extension of work done by [4,5], Bachok et al. [7] and Adnan et al. [41]. The purpose of this study is to propose a new model that investigates the behavior of the flow and heat transfer for an unsteady stagnation-point flow over an exponential stretching/shrinking sheet in the presence of suction/injection and the velocity slip parameter immersed in nanofluid. The nanofluid model proposed by Tiwari and Das was chosen to study the effect of nanoparticle volume fraction towards the skin friction coefficient and heat transfer coefficient. Other parameter effects that have been considered in this study are the unsteadiness parameter, velocity slip, suction/injection,

and types of nanoparticles, i.e., Copper, Alumina, and Titania, in water as the base fluid. The system is transformed to ordinary differential equations and has been solved numerically using the boundary value problem with fourth order accuracy (bvp4c) function in Matlab. The numerical results are presented graphically for the tested parameters. Finally, the stability analysis has to be done to find a stable and realizable solution for numerical results which have dual solutions.

### 2. Mathematical Formulation

The system of two-dimensional laminar incompressible unsteady stagnation-point flow (density is constant), permeable surface, stretching/shrinking sheet in the water as the base fluid with different types of nanoparticles, i.e., Copper, Alumina, and Titania, is studied, as the Tiwari and Das model is considered. Let the unsteady free stream velocity be  $U_\infty = (a/(1 - ct))e^{x/l}$ ,  $a$  is the stagnation length, and  $c$  is the flow unsteadiness parameter. Assume that the plate velocity is  $u_w = \varepsilon(a/(1 - ct))e^{x/l}$  where  $\varepsilon > 0$  for stretching velocity rate,  $\varepsilon < 0$  for shrinking velocity rate,  $l$  is the characteristic length, and  $v_w = v_0e^{x/2l}/(1 - ct)$  represents mass flux velocity with  $v_0$  as a constant. Let the slip occur between the fluid and the surface, which is represented as  $u_s = L\partial u/\partial y$ , where  $L$  is the slip length (see Bhattacharyya et al. [8]). The reference temperature, ambient temperature, and temperature distribution near the surface are  $T_0, T_\infty$  and  $T_w = T_\infty + (T_0/(1 - ct))e^{x/2l}$ , where both  $T_0$  and  $T_\infty$  are constants. Apart from that, the  $x$ -axis is parallel to stream direction while the  $y$ -axis is perpendicular to it. A schematic diagram of the problem is shown in Figure 1.

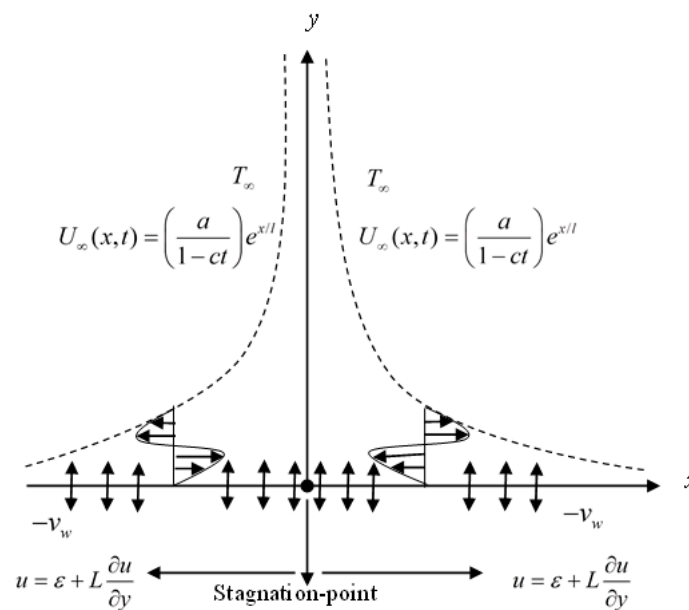


Figure 1. Schematic diagram of the problem.

Based on the above assumptions, the governing equations can be written as follows (see Zaib et al. [4] and Bachok et al. [7]):

$$\frac{\partial u}{\partial x} + \frac{\partial v}{\partial y} = 0, \tag{1}$$

$$\frac{\partial u}{\partial t} + u \frac{\partial u}{\partial x} + v \frac{\partial v}{\partial y} = \frac{\partial U_\infty}{\partial t} + U_\infty \frac{\partial U_\infty}{\partial x} + \frac{\mu_{nf}}{\rho_{nf}} \frac{\partial^2 u}{\partial y^2}, \tag{2}$$

$$\frac{\partial T}{\partial t} + u \frac{\partial T}{\partial x} + v \frac{\partial T}{\partial y} = \alpha_{nf} \frac{\partial^2 T}{\partial y^2}, \tag{3}$$

subject to boundary conditions

$$v = -v_w, u = \varepsilon + L \frac{\partial u}{\partial y}, T = T_w \quad \text{at } y = 0, \tag{4}$$

$$u \rightarrow U_\infty, T \rightarrow T_\infty \quad \text{as } y \rightarrow \infty.$$

where  $u$  and  $v$  are velocity component in  $x$  and  $y$  axes respectively,  $t$  denotes time  $v_w = v_0 e^{x/2l} / (1 - ct)^{1/2}$  is the variable suction velocity with  $v_0 > 0$  being a constant,  $T$  is the nanofluid temperature,  $\mu_{nf}, \alpha_{nf}, k_{nf}$  and  $(\rho c_p)_{nf}$  represent the viscosity, thermal diffusivity, thermal conductivity and heat capacity of the nanofluid, respectively. Equation (5) is given by Oztop et al. [42]:

$$\mu_{nf} = \frac{\mu_f}{(1 - \varphi)^{2.5}}, \tag{5}$$

$$\alpha_{nf} = \frac{k_{nf}}{(\rho c_p)_{nf}}, \tag{6}$$

$$\frac{k_{nf}}{k_f} = \frac{k_s + 2k_f - 2\varphi(k_f - k_s)}{k_s + 2k_f + \varphi(k_f - k_s)}, \tag{7}$$

$$(\rho c_p)_{nf} = (\rho c_p)_f \left[ 1 - \varphi + \varphi \left( \frac{(\rho c_p)_s}{(\rho c_p)_f} \right) \right], \rho_{nf} = \rho_f \left[ 1 - \varphi + \varphi \left( \frac{\rho_s}{\rho_f} \right) \right], \tag{8}$$

where  $\varphi$  denotes the volume of the nanoparticle,  $\mu_f$  is the viscosity of the fluid,  $(\rho C_p)_{nf}, (\rho C_p)_s$  and  $(\rho C_p)_f$  is the heat capacity of the nanofluid, nanoparticle and fluid  $k_s$  and  $k_f$  are the thermal conductivities of the nanoparticle and fluid, respectively. The densities of the fluid and nanoparticle are denoted as  $\rho_f$  and  $\rho_s$ , respectively.

The system of ordinary differential Equations (1)–(3) bounded by (4) is transformed to the simpler form by using the similarity transformation variables, which are given by:

$$\eta = \left( \frac{a}{2lv_f(1 - ct)} \right)^{1/2} e^{x/2l} y, \psi = \left( \frac{2lv_f a}{1 - ct} \right)^{1/2} e^{x/2l} f(\eta), \theta(\eta) = \frac{T - T_\infty}{T_w - T_\infty}. \tag{9}$$

The stream function  $\psi$  is defined as  $u = \partial\psi/\partial y$  and  $v = -\partial\psi/\partial x$ , where

$$\partial\psi/\partial y = \left( \frac{a}{1 - ct} \right) e^{x/2l} f'(\eta) \text{ and } -\partial\psi/\partial x = -\left( \frac{v_f a}{2l(1 - ct)} \right)^{1/2} e^{x/2l} (f(\eta) + \eta f'(\eta)) \tag{10}$$

satisfies the continuity Equation (1). Further, Equations (2) and (3), subjected to the boundary conditions (4), are transformed into the following Equations (11)–(13):

$$\frac{1}{(1 - \varphi)^{2.5} \left( 1 - \varphi + \varphi \left( \frac{\rho_s}{\rho_f} \right) \right)} f''' + ff'' - 2f'^2 + 2 - A(2f' + \eta f'' - 2) = 0, \tag{11}$$

$$\frac{1}{Pr} \frac{k_{nf}}{k_f \left( 1 - \varphi + \varphi \left( \frac{(\rho c_p)_s}{(\rho c_p)_f} \right) \right)} \theta'' + f\theta' - f'\theta - A(2\theta + \eta\theta') = 0, \tag{12}$$

subject to boundary conditions:

$$f(0) = s, f'(0) = \varepsilon + \sigma f''(0), \theta(0) = 1 \text{ at } \eta = 0, \tag{13}$$

$$f'(\eta) \rightarrow 1, \theta(\eta) \rightarrow 0 \text{ as } \eta \rightarrow \infty.$$

Primes denote the differentiation with respect to  $\eta$ ,  $\sigma = L\left(a/2lv_f(1-ct)\right)^{1/2} e^{x/2l}$  is the slip velocity parameter,  $Pr = v_f/\alpha_f$  is the Prandtl number, and  $A = cl/ae^{x/l}$  is the dependent unsteadiness parameter,  $s = v_0\left(2l/av_f\right)^{1/2} > 0$  representing the suction parameter;  $s = v_0\left(2l/av_f\right)^{1/2} < 0$  is an injection parameter.

The physical quantities of interest are the local skin friction coefficient  $C_f$  and local Nusselt number  $Nu_x$ , which are given by Equation (14) (see Rao et al. [5]):

$$C_f = \frac{\tau_w}{\rho_f U_\infty^2}, Nu_x = \frac{lq_w}{k_f(T_w - T_\infty)}, \tag{14}$$

where  $\tau_w$  is the shear stress and  $q_w$  is the heat flux at the surface which is represented by Equation (15).

$$\tau_w = \mu_{nf} \left(\frac{\partial u}{\partial y}\right)_{y=0}, q_w = -k_{nf} \left(\frac{\partial T}{\partial y}\right)_{y=0}, \tag{15}$$

Using (9), (14), and (15), both  $C_f Re_x^{1/2}$  and  $Nu_x Re_x^{-1/2}$  are given by Equations (16) and (17), respectively.

$$C_f(2Re_x)^{1/2} = \frac{1}{(1-\varphi)^{2.5}} f''(0), \tag{16}$$

$$Nu_x \left(\frac{2}{Re_x}\right)^{1/2} = -\frac{k_{nf}}{k_f} \theta'(0), \tag{17}$$

where  $Re_x = U_\infty l/v_f$  denotes the local Reynolds number.

### 3. Stability Analysis

The results display the presence of dual solutions for the tested parameter. Due to the importance of identifying the physically-realizable solution, a stability analysis is performed. Following Merkin [30], a new dimensionless variable,  $\tau$ , is introduced, which is related to an initial value problem. The new dimensionless variables can be represented in Equation (18):

$$\eta = \left(\frac{a}{2lv_f(1-ct)}\right)^{1/2} e^{x/2l} y, \psi = \left(\frac{2lv_f a}{1-ct}\right)^{1/2} e^{x/2l} f(\eta, \tau), \theta(\eta, \tau) = \frac{T-T_\infty}{T_w-T_\infty}, \tag{18}$$

$$\tau = \frac{at}{2l(1-ct)} e^{x/l}.$$

Equation (18) is then substituted into (2) and (3) to obtain

$$\frac{1}{(1-\varphi)^{2.5} \left(1-\varphi+\varphi\left(\frac{\rho_s}{\rho_f}\right)\right)} \frac{\partial^3 f}{\partial \eta^3} + f \frac{\partial^2 f}{\partial \eta^2} - 2\left(\frac{\partial f}{\partial \eta}\right)^2 + 2 - A\left(2\frac{\partial f}{\partial \eta} + \eta \frac{\partial^2 f}{\partial \eta^2} - 2\right) - \left(2\tau \frac{\partial f}{\partial \eta} + 2A\tau + 1\right) \frac{\partial^2 f}{\partial \eta \partial \tau} = 0, \tag{19}$$

$$\frac{1}{Pr} \frac{k_{nf}}{k_f \left(1-\varphi+\varphi\left(\frac{\rho_c p_s}{\rho_c p_f}\right)\right)} \frac{\partial^2 \theta}{\partial \eta^2} + f \frac{\partial \theta}{\partial \eta} - \theta \frac{\partial f}{\partial \eta} - A\left(2\theta + \eta \frac{\partial \theta}{\partial \eta}\right) - (1+2A\tau+2\tau) \frac{\partial \theta}{\partial \tau} = 0, \tag{20}$$

along with the boundary conditions:

$$f(0, \tau) = s, \frac{\partial f}{\partial \eta}(0, \tau) = \varepsilon + \sigma \frac{\partial^2 f}{\partial \eta^2}(0, \tau), \theta(0, \tau) = 1, \tag{21}$$

$$\frac{\partial f}{\partial \eta}(\eta, \tau) \rightarrow 1, \theta(\eta, \tau) \rightarrow 0, \text{ as } \eta \rightarrow \infty.$$

The stability of solutions  $f(\eta) = f_0(\eta)$  and  $\theta(\eta) = \theta_0(\eta)$  that satisfy the boundary value problem Equations (11)–(13) is tested by introducing (see Merkin [30] and Weidman et al. [31]):

$$f(\eta, \tau) = f_0(\eta) + e^{-\gamma \tau} F(\eta, \tau) \text{ and } \theta(\eta, \tau) = \theta_0(\eta) + e^{-\gamma \tau} G(\eta, \tau), \tag{22}$$

where  $\gamma$  is an unknown eigenvalue parameter,  $F(\eta, \tau)$  and  $G(\eta, \tau)$  are small corresponding to  $f_0(\eta)$  and  $\theta_0(\eta)$ , respectively.

The linearized problem can be obtained by substituting Equation (22) into (19) and (20), as below:

$$\frac{1}{(1-\varphi)^{2.5} \left(1-\varphi+\varphi\left(\frac{\rho_s}{\rho_f}\right)\right)} \frac{\partial^3 F}{\partial \eta^3} + f_0 \frac{\partial^2 F}{\partial \eta^2} + F f_0'' - 4f_0' \frac{\partial F}{\partial \eta} - A\eta \frac{\partial^2 F}{\partial \eta^2} \tag{23}$$

$$-2A \frac{\partial F}{\partial \eta} - 2A \frac{\partial^2 F}{\partial \eta \partial \tau} + 2A\gamma \frac{\partial F}{\partial \eta} \frac{\partial^2 F}{\partial \eta \partial \tau} + \gamma \frac{\partial F}{\partial \eta} - 2\tau \frac{\partial^2 F}{\partial \eta \partial \tau} + 2\tau\gamma \frac{\partial F}{\partial \eta} = 0,$$

$$\frac{1}{Pr} \frac{k_{nf}}{k_f \left(1-\varphi+\varphi\left(\frac{(\rho c_p)_s}{(\rho c_p)_f}\right)\right)} \frac{\partial^2 G}{\partial \eta^2} - A\eta \frac{\partial G}{\partial \eta} - 2A\tau \frac{\partial G}{\partial \tau} - 2A\tau\gamma G - \frac{\partial G}{\partial \tau} + \gamma G \tag{24}$$

$$-2AG - 2\tau f_0' \frac{\partial G}{\partial \tau} + \gamma 2\tau f_0' G - \theta_0 \frac{\partial F}{\partial \eta} - f_0' G + \theta_0' F + f_0 \frac{\partial G}{\partial \eta} = 0,$$

subject to boundary conditions

$$F(0, \tau) = 0, \frac{\partial F(0, \tau)}{\partial \eta} + \sigma \frac{\partial^2 F(0, \tau)}{\partial \eta^2} = 0, G(0, \tau) = 0, \tag{25}$$

$$\frac{\partial F(\eta, \tau)}{\partial \eta} \rightarrow 0, G(\eta, \tau) \rightarrow 0 \text{ as } \eta \rightarrow \infty.$$

The stability of the steady flow  $f_0(\eta)$  and  $\theta_0(\eta)$  can be tested by setting  $\tau = 0$ , for which  $F(\eta) = F_0(\eta)$  and  $G(\eta) = G_0(\eta)$  are obtained, indicating the initial growth or decay as in Equation (22). Hence, the linearized problem (23) and (25) can be written as:

$$\frac{1}{(1-\varphi)^{2.5} \left(1-\varphi+\varphi\left(\frac{\rho_s}{\rho_f}\right)\right)} F_0''' + f_0 F_0'' + F_0 f_0'' - 4f_0' F_0' - A\eta F_0'' + (\gamma - 2A) F_0' = 0, \tag{26}$$

$$\frac{1}{Pr} \frac{k_{nf}}{k_f \left(1-\varphi+\varphi\left(\frac{(\rho c_p)_s}{(\rho c_p)_f}\right)\right)} G_0'' - A\eta G_0' - 2AG_0 - \theta_0 F_0' - f_0' G_0 + \theta_0' F_0 + f_0 G_0' + \gamma G_0 = 0, \tag{27}$$

along with boundary conditions

$$F_0(0) = 0, F_0'(0) - \sigma F_0''(0) = 0, G_0(0) = 0, \tag{28}$$

$$F_0'(\eta) \rightarrow 0, G_0(\eta) \rightarrow 0 \text{ as } \eta \rightarrow \infty.$$

The possible range of the smallest eigenvalues can be found by relaxing a boundary condition of  $F_0(\eta)$  or  $G_0(\eta)$  from condition  $\eta \rightarrow \infty$  as proposed by Harris et al. [32]. In this paper, it was decided that  $F_0'(\eta) \rightarrow 0$  should be relaxed, and the new boundary condition will be replaced by  $F_0''(0) = 1$ .

#### 4. Numerical Methodology

The dual solutions of the ordinary Equations (11) and (12), along with the boundary conditions (13), are found using the bvp4c program in the Matlab software (Software, MathWorks, MA, USA). The program is a finite-different code which applies the three-stage Labatto IIIa formula and its algorithm, depending on an iteration structure, in solving the system of equations. The collocation of formulas and polynomials gives a C1-continuous solution with fourth-order accuracy. In this program, the missing values of the skin friction coefficient  $f''(0)$  and heat transfer coefficient  $-\theta'(0)$  are found by setting some values of initial guesses for the different tested parameters, and asymptotically fulfilled

the far-field boundary conditions. The finding process is repeated until no more solutions can be found either beyond a point, namely, the critical point  $\epsilon_c$ , or for a certain domain if the critical point is hard to find, or the point does not actually exist. Some points near the critical values for the first and second solutions are then tested using the stability analysis to find the smallest eigenvalues,  $\gamma$ , to determine the stability of the solutions. The smallest eigenvalues can be found by solving the linearized problem (26)–(28) using the same program for both the upper and lower solutions. Positive eigenvalue indicate that the solution is stable, while negative values shows an unstable solution.

### 5. Results and Discussion

The effects of the nanoparticle volume fraction  $\varphi$ , velocity slip parameter  $\sigma$ , unsteadiness parameter  $A$ , stretching/shrinking parameter  $\epsilon$ , suction/injection parameter  $s$ , and different types of nanoparticles (Copper, Alumina, and Titania) are studied, and have been displayed in Figures 1–10. As suggested in the Tiwari and Das model, water with a Prandtl number of 6.2 ( $Pr = 6.2$ ) was chosen as the base fluid, and the value of the nanoparticle volume fraction was between 0 and 0.2 ( $0 \leq \varphi \leq 0.2$ ), where the absence of nanoparticles in the base fluid can be known when  $\varphi = 0$ . The thermo physical properties of water, Copper, Alumina, And Titania are tabulated in Table 1, for which the value of each substance is taken from Oztop and Abu-Nadda [42]. Validation has been made from previous work by Bachok et al. [7], whereby the steady problem ( $A = 0$ ) over a permeable surface ( $s = 0$ ) with no-slip condition ( $\sigma = 0$ ) was considered, as shown in Table 2; we observed excellent agreement.

**Table 1.** Thermo physical properties of water, Copper, Alumina, and Titania (see Oztop and Abu-Nadda [42]).

Substance	Density, $\rho$ (kg/m <sup>3</sup> )	Specific Heat, $C_p$ (J/kg·K)	Conductivity, $K$ (W/m·K)
Water	997.1	4179	0.613
Copper	8933	385	400
Alumina	3970	765	40
Titania	4250	686.2	8.9538

**Table 2.** Values of  $f''(0)$  and  $-\theta'(0)$  for different values of  $\epsilon$  and  $\varphi$  for Cu-water.

$\epsilon$	$\varphi$	Bachok et al. [7]		Present Results	
		$f''(0)$	$-\theta'(0)$	$f''(0)$	$-\theta'(0)$
−0.5	0	2.1182	0.687	2.1182	0.6870
	0.1	3.2381	1.1432	3.2330	1.1400
	0.2	4.5071	1.5184	4.5009	1.5151
0	0	1.6872	1.7148	1.6872	1.7148
	0.1	2.5794	2.1358	2.5793	2.1358
	0.2	3.5901	2.5400	3.5901	2.5400
0.5	0	0.9600	2.4874	0.9604	2.4874
	0.1	1.4682	2.915	1.4682	2.9150
	0.2	2.0436	3.3565	2.0436	3.3565

The effects of the nanoparticle volume fraction  $\varphi$  on the skin friction coefficient  $f''(0)$  and heat transfer coefficient  $-\theta'(0)$  with stretching/shrinking parameter  $\epsilon$  in Copper-water nanofluid are depicted in Figure 2. Both figures show that dual solutions can be obtained when  $\epsilon_c \leq \epsilon$ , while no solution can be found when  $\epsilon < \epsilon_c$ , i.e., where the critical point  $\epsilon_c$  represents the end point of the existed solution. The range of solutions was shown to widen when the amount of Copper nanoparticles in the water increases. Apart from that, the skin friction coefficient  $f''(0)$  for both solutions in the shrinking surface was found to be higher than in the stretching surface, while the heat transfer coefficient shows the opposite trend. Moreover, increasing the volume fraction of Copper nanoparticles in

water increases the skin friction coefficient for the first solution, but decreases the second solution. Meanwhile, for the heat transfer coefficient, increasing  $\varphi$  shows a decreasing trend for both solutions.

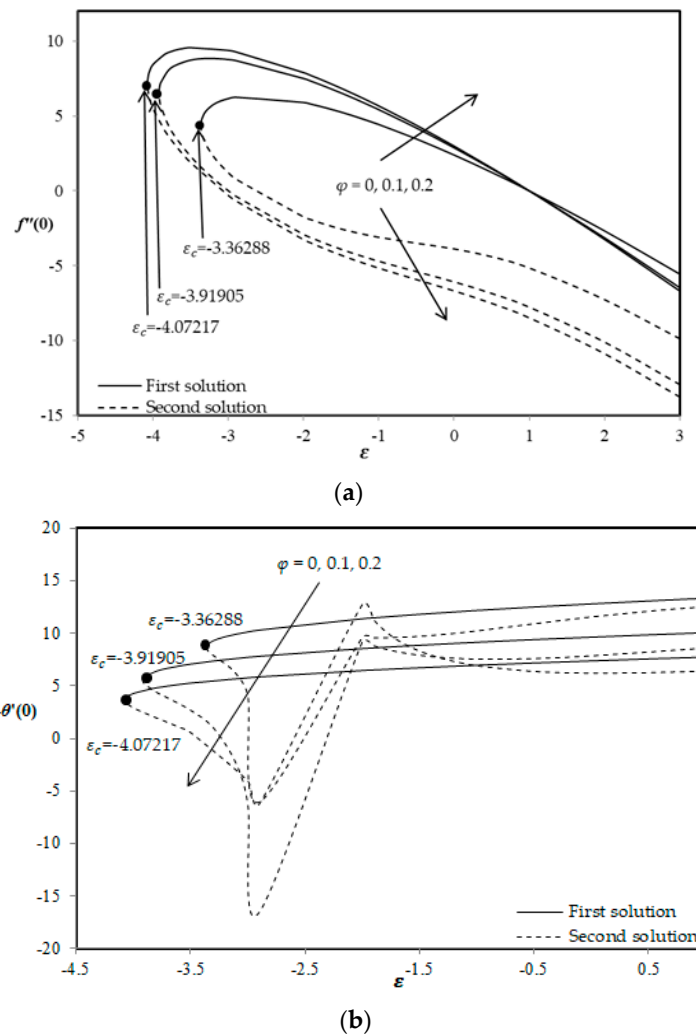
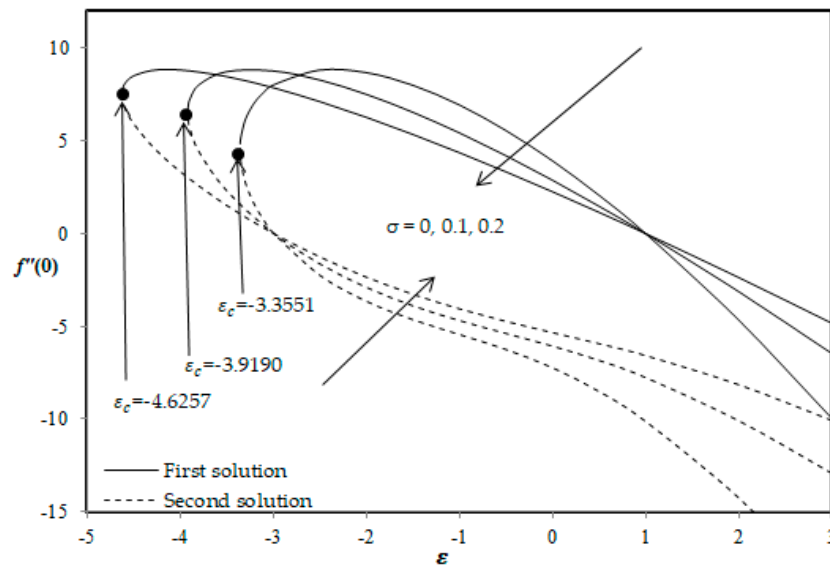
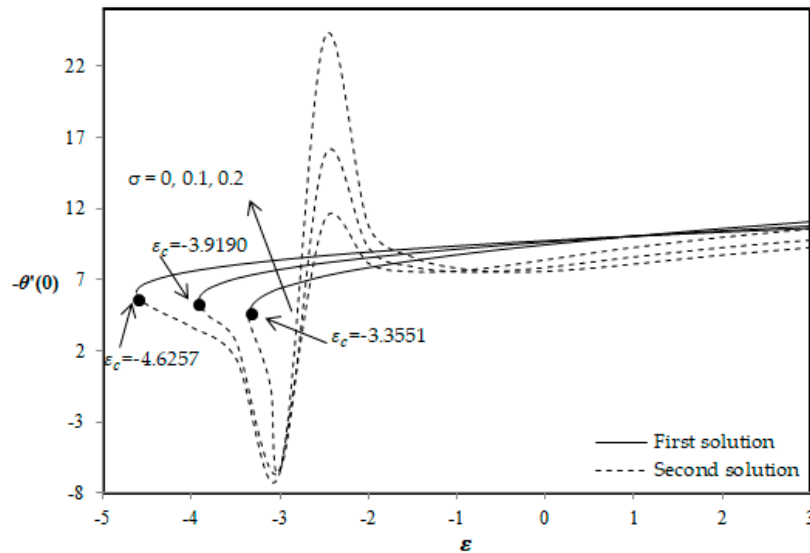


**Figure 2.** (a) Skin friction coefficient and (b) Local Nusselt number for different  $\varphi$  in Copper-water nanofluid with  $\varepsilon$  when  $s = 2, \sigma = 0.1$  and  $A = 0.1$ .

Figure 3 display the effect of different slip parameters on the skin friction coefficient  $f''(0)$  and heat transfer coefficient  $-\theta'(0)$  with stretching/shrinking parameter  $\varepsilon$  in a Copper water nanofluid. Based on the figures, dual solutions exist when  $\varepsilon_c \leq \varepsilon$ , while no solution could be reported for  $\varepsilon < \varepsilon_c$ . It can also be observed that as the slip effect becomes higher, the range of solutions is consequently expanded, also decreasing the skin friction coefficient  $f''(0)$  for the first solution, but increasing it for the second solution within the range  $\varepsilon < 1$ . The heat transfer coefficient  $-\theta'(0)$  showed an uptrend for the first solution and downward one for the second, as the velocity slip  $\sigma$  increases. In addition, the skin friction coefficient for the shrinking surface was found higher than  $f''(0)$  for the stretching surface. It can be observed that the heat transfer coefficient  $-\theta'(0)$  for the shrinking surface is slightly decreased compared to that of the stretching surface. Hence, the friction between the nanofluid and the surface is larger when the surface is shrunk compared to the stretched surface. Meanwhile, based on Figure 3b, the heat transfer rate at the surface was found to be faster for a stretching surface than a shrinking surface; thus, the cooling process becomes better when the surface is in stretched state.



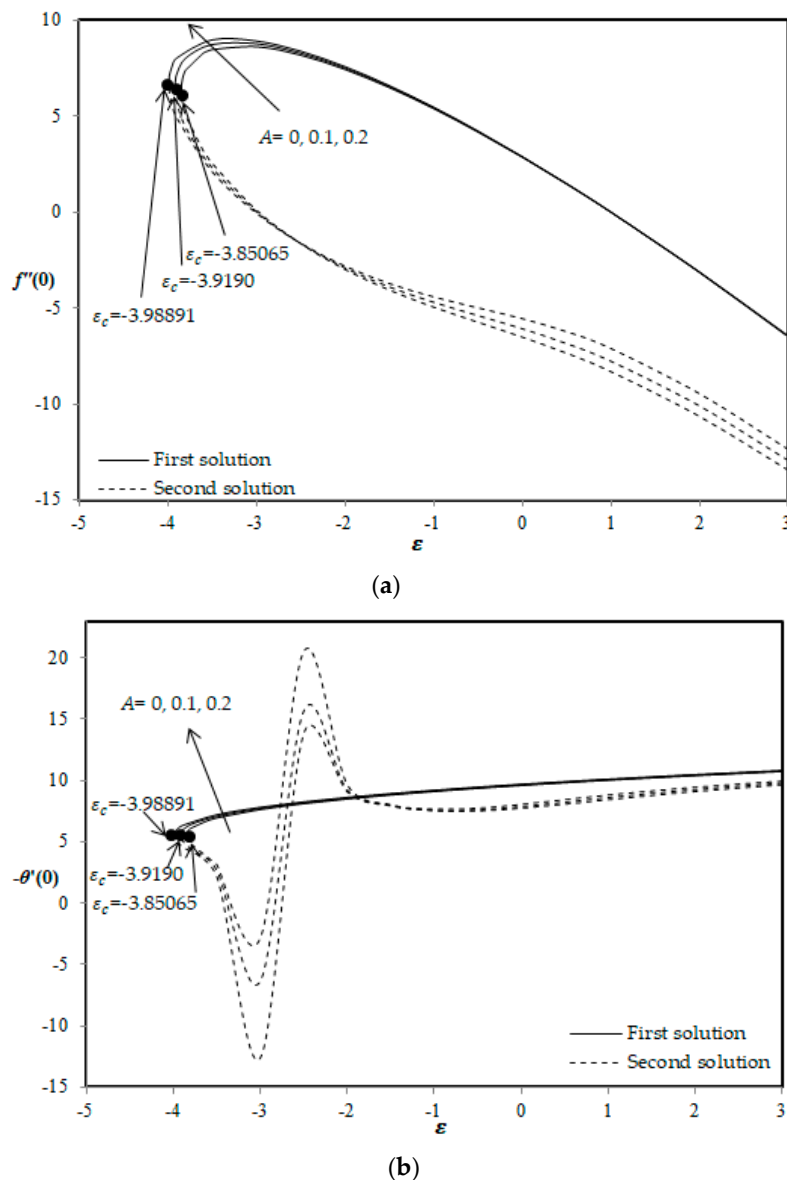
(a)



(b)

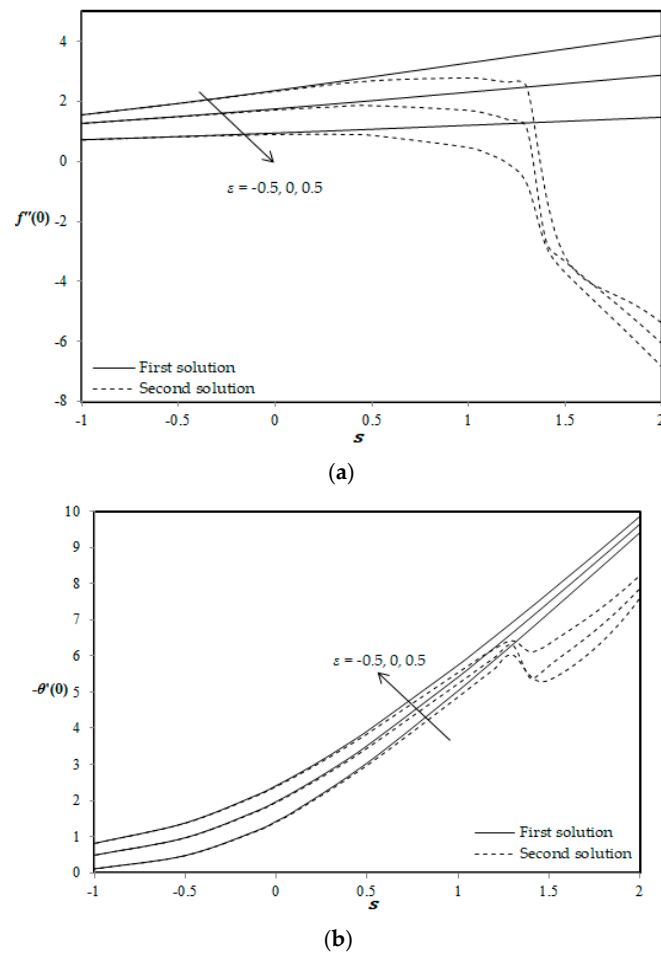
**Figure 3.** (a) Skin friction coefficient and (b) Local Nusselt number for different  $\sigma$  with  $\epsilon$  in Copper-water nanofluid when  $s = 2$ ,  $\sigma = 0.1$  and  $A = 0.1$ .

Variations of the skin friction coefficient  $f''(0)$  and heat transfer coefficient  $-\theta'(0)$  due to the effect of unsteadiness of parameter  $A$  with stretching/shrinking surfaces, are shown in Figure 4. In the range of  $\epsilon_c \leq \epsilon$ , dual solutions can be found, while no solution may be obtained when  $\epsilon_c > \epsilon$ . According to these figures, the unsteadiness parameter  $A$  only expanded the range of solutions slightly compared to the effects of the nanoparticle volume fraction  $\phi$  and the velocity slip parameter  $\sigma$ . Increasing the unsteadiness parameter  $A$  increases the skin friction coefficient for the first solution, and decreases if for the second. In addition, as  $A$  increases, the heat transfer rate at the surface for the first solution is also increased, but the second solution shows the opposite behavior. The skin friction coefficient  $f''(0)$  was shown to decrease when the value of  $\epsilon$  increases, which indicates that the skin friction over a shrinking surface is higher than that over a stretching surface. In the meantime, the heat transfer coefficient  $-\theta'(0)$  increases slightly when  $\epsilon$  increases, which shows that the heat transfer rate for the shrinking surface is higher than that of the stretching surface.



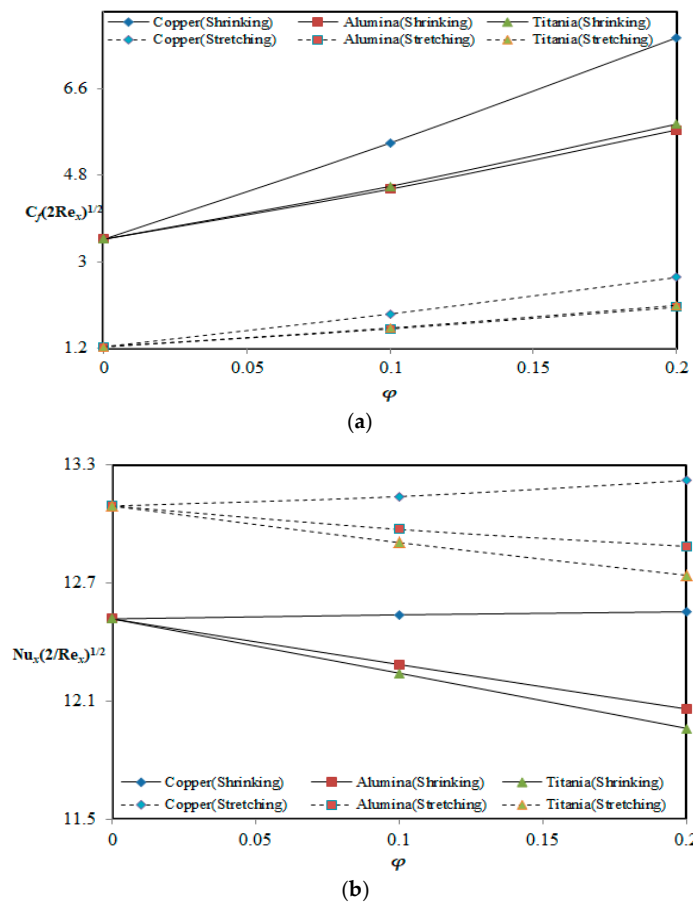
**Figure 4.** (a) Skin friction coefficient and (b) Local Nusselt number for different  $A$  with  $\epsilon$  in Copper-water nanofluid when  $s = 2, \sigma = 0.1$  and  $\phi = 0.1$ .

Figure 5 is presented in order to show the effect of the  $\epsilon$  parameter with the suction/injection parameter on the skin friction coefficient as  $f''(0)$ , and the heat transfer coefficient  $-\theta'(0)$  where the dual solutions are obtained for a permeable surface ( $s > 0$  and  $s < 0$ ) and an impermeable surface ( $s = 0$ ). Figure 5a shows the decreasing skin friction coefficient for the first and second solutions when the value of  $\epsilon$  is increased. This indicates that the resulting skin friction coefficient for the shrinking case is higher than that of the skin friction coefficient, which is caused in the stretching case by either a permeable or an impermeable surface. Figure 5b displays the opposite trend, where the heat transfer coefficient increases as  $\epsilon$  increases for both solutions. This indicates that the heat transfer rate over shrinking surface is higher than that over a stretching surface for each  $s$  parameter. In addition, it is clearly seen in Figure 5 that the solution for the second solution was easier to find with a higher value of  $s$ . Furthermore, as the effect of the suction parameter ( $s > 0$ ) becomes stronger, or the effect of injection parameter ( $s < 0$ ) becomes weaker, the skin friction coefficient increases for the first and second solutions ( $s < 1.5$ ), and the heat transfer coefficient increases for both solutions.



**Figure 5.** (a) Skin friction coefficient and (b) Local Nusselt number for different  $\epsilon$  with  $s$  in Copper-water nanofluid when  $A = 0.1, \sigma = 0.1$  and  $\varphi = 0.1$ .

Figures of local skin friction coefficient  $C_f(2Re_x)^{1/2}$  and local Nusselt number  $Nu(2/Re_x)^{1/2}$  from Equations (16) and (17) are illustrated in Figure 6 with different nanoparticle types, namely, Copper, Alumina, and Titania, for various nanoparticle volume fractions in the base fluid ( $0 \leq \varphi \leq 0.2$ ) over both stretching ( $\epsilon > 0.5$ ) and shrinking ( $\epsilon < 0.5$ ) surfaces. The local skin friction for the shrinking surface is much higher than that over the stretching surface, which indicates that the shear stress between the surface and fluid is larger for the flow over a shrinking sheet than a stretching sheet. Meanwhile, the local Nusselt number for the stretching surface is obviously higher than that for the shrinking surface. This denotes that the heat transfer rate at the surface is greater when the sheet is stretched. The increasing of nanoparticle volume fraction from 0 to 0.2 in water affects both the local skin friction coefficient as well as the local Nusselt number, where it increases the local skin friction for each nanoparticle over both stretching and shrinking surfaces. However, only the Copper-water nanofluid showed an increase in transferring the heat at the surface; the two other types of studied nanoparticles, Alumina and Titania, caused a decrease in the value for the local Nusselt number. These figures also show that different types of nanoparticles have a significant affect on shear stress and the heat transfer rate at the surface. The Copper-water nanofluid was found to have the highest local skin friction coefficient and local Nusselt number for each value of the nanoparticle volume fraction over both surfaces. This means that the Copper-water nanofluid causes larger shear stress at the surface, and also has the ability to transfer heat at the surface more effectively than Titania and Alumina, since Copper has the highest thermal conductivity, as can be seen in Table 1.



**Figure 6.** (a) Skin friction coefficient and (b) Local Nusselt number for different  $\varepsilon$  with  $s$  in Copper-water nanofluid when  $A = 0.1, \sigma = 0.1$  and  $\varphi = 0.1$ .

The profiles of velocity and temperature of the fluid for different values of  $\sigma, \varepsilon$ , and  $s$  are displayed in Figures 7–10 in order to support the results from Figures 2–6, where dual solutions are obtained. These profiles also are depicted to show that the far field boundary conditions from Equation (13) are asymptotically fulfilled. Each profile illustrates that the velocity and thermal boundary layer thicknesses for the first solution are smaller than for the second solution for every tested parameter, implying that the second solution is unstable, as mentioned by Bachok et al. [7]. Figure 7a shows that by increasing  $\sigma$ , the fluid velocity increases for the first solution but decreases for the second. Meanwhile, Figure 7b presents the opposite behaviour, i.e., where the thermal boundary layer thickness is decreasing for the first solution and increasing for the second as the slip parameter becomes more significant. Therefore, the presence of velocity slip between the fluid and the surface accelerates the flow of the fluid, which decreases the deficiency between the velocity in the ambient flow and in the boundary layer. In addition, the consideration of velocity slip in real life applications is one means of reducing the skin friction coefficient at the surface, and can extend the lifetime of the material because it delays the corrosion process. The velocity and temperature profiles for a stretching surface ( $\varepsilon = 0.5$ ), shrinking surface ( $\varepsilon = -0.5$ ) and static surface ( $\varepsilon = 0$ ) are shown in Figure 8a,b. The velocity for the stretching case is seen to be higher than other cases for both solutions. In contrast, the temperature for the stretching surface is lower than that for shrinking and static surfaces for the first and second solutions. Physically, the stretching surface increases the velocity of the fluid, decreases the energy capability, and postpones the heat from spread up. The effects of different values of  $s$  on the velocity and temperature profiles are also displayed in Figures 9 and 10 for both stretching and shrinking sheets. According to Figures 9a and 10a, the velocity profile for the suction case  $s = 1$  is higher than that for the injection case  $s = -1$ , as well as over the impermeable surface  $s = 0$  for the first solution,

showing the opposite behaviour for the second solution. Figures 9b and 10b display the decreasing temperature profile as the value of  $s$  rises for both solutions, which indicates that the heat transfer rate at the surface becomes higher, and leads to a reduction in the temperature for the mass injection case compared to the mass suction case.

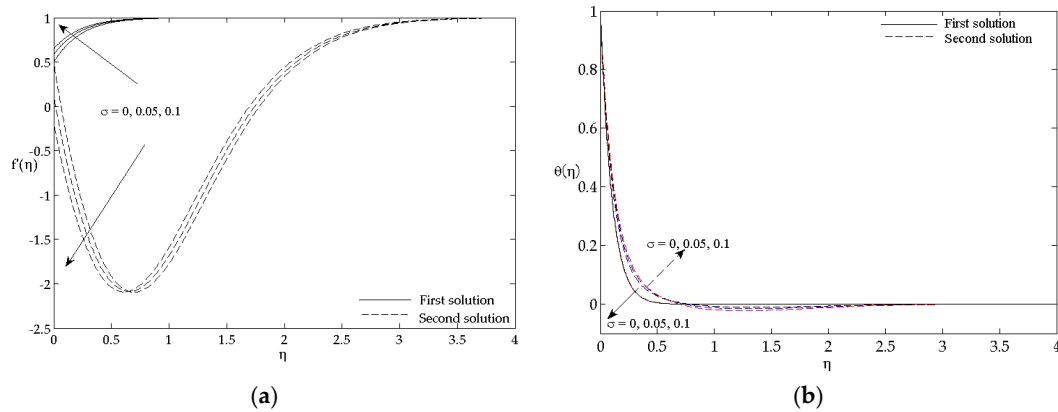


**Figure 7.** (a) Velocity profile and (b) Temperature profile for different  $\sigma$  in Copper-water nanofluid when  $\varepsilon = 0.5$ ,  $\varphi = 0.1$ ,  $s = 2$  and  $A = 0.1$ .

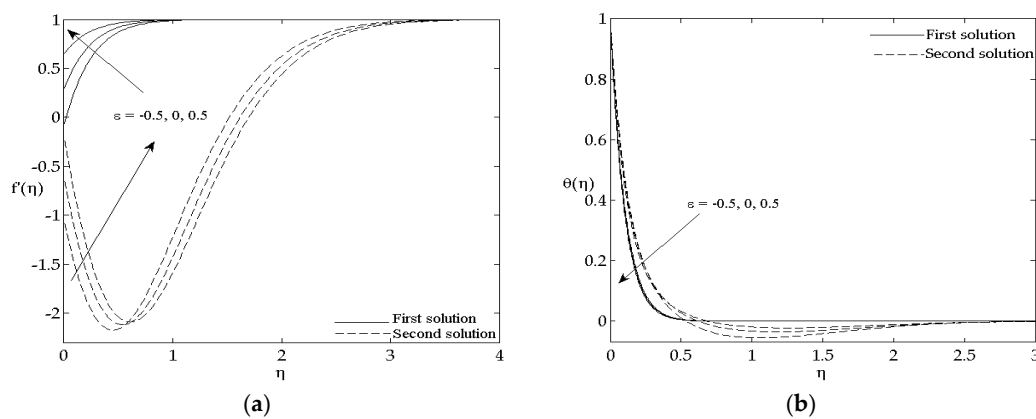


**Figure 8.** (a) Velocity profile and (b) Temperature profile for different  $\varepsilon$  in Copper-water nanofluid when  $\sigma = 0.1$ ,  $\varphi = 0.1$ ,  $s = 2$  and  $A = 0.1$ .

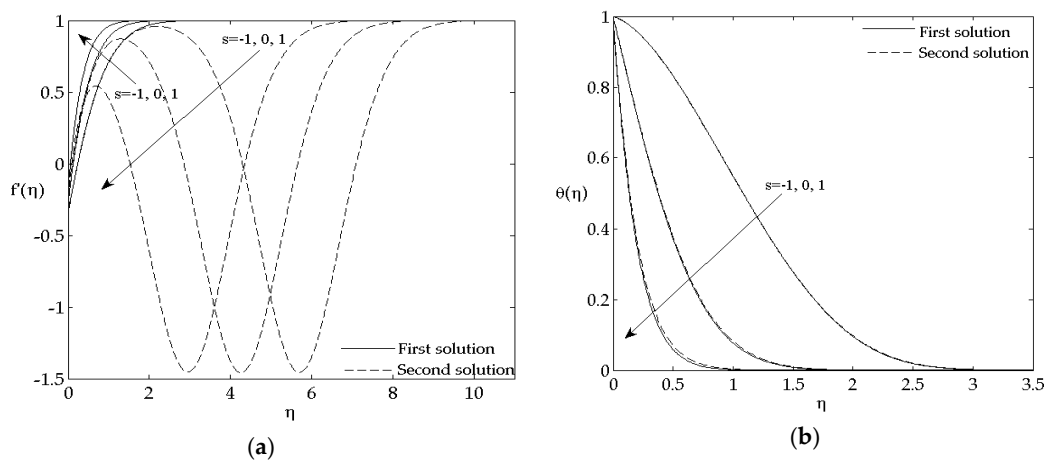


**Figure 9.** (a) Velocity profile and (b) Temperature profile for different  $s$  in Copper-water nanofluid when  $\sigma = 0.1$ ,  $\varphi = 0.1$ ,  $A = 0.1$  and  $\varepsilon = -0.5$  (shrinking).

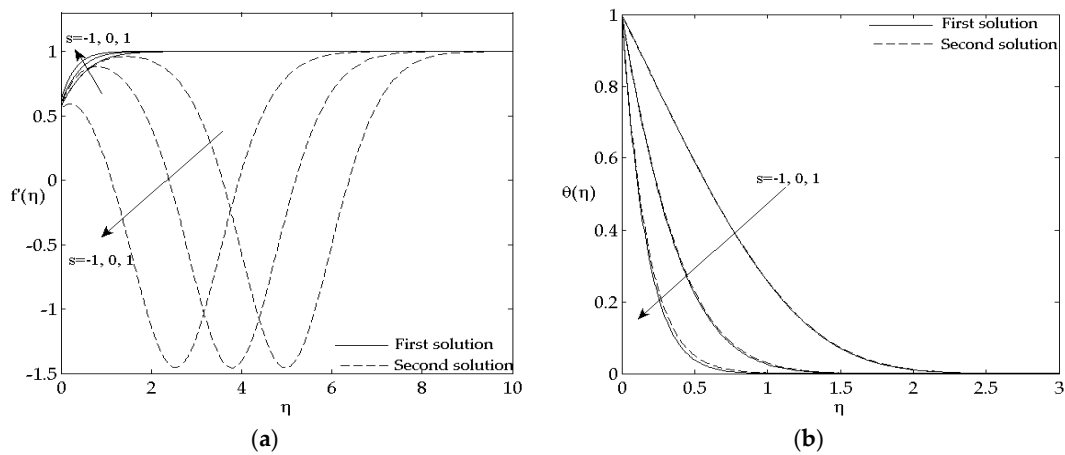


**Figure 10.** (a) Velocity profile and (b) Temperature profile for different  $s$  in Copper-water nanofluid when  $\sigma = 0.1$ ,  $\varphi = 0.1$ ,  $A = 0.1$  and  $\varepsilon = 0.5$  (stretching).

Since dual solutions are obtained, a stability analysis is implemented to identify the stability of the two solutions. According to the aforementioned authors, the upper solution is considered stable, and the solution from the first solution is physically realizable. However, the second solution is considered unstable, and is not physically realizable in real life applications. The stability of each solution is determined by the value of the smallest eigenvalue  $\gamma$  regardless of whether the value is positive or negative. A positive value of  $\gamma$  indicates that there is initial decay of the disturbance in the solution, meaning that the solution with a positive value is stable. On the other hand, a negative eigenvalue represents an initial growth of disturbance, causing the solution to become unstable. Table 3 shows the smallest eigenvalues for the upper and lower solutions for different nanoparticle volume fractions,  $\varphi$ , and for some values of shrinking parameter  $\varepsilon < 0$  where these values are close to the critical values  $\varepsilon_c$  for each case. Based on the table, the smallest eigenvalues for the upper (first) solution are positive, while negative values are obtained for the smallest eigenvalues from the lower (second) solution. Therefore, the first solution is stable, and the results obtained are physically realizable, while those of the second solution are not.

**Table 3.** The smallest eigenvalues  $\gamma$  for different nanoparticle volume fraction  $\varphi$  with various values of  $\varepsilon$ .

$\varphi$	$\varepsilon$	$\gamma$ Upper	$\gamma$ Lower
0.0	-3.36287	0.014484	-0.014485
	-3.36286	0.021581	-0.021578
	-3.36285	0.026868	-0.026858
0.1	-3.91902	0.04267	-0.042654
	-3.91901	0.045607	-0.04558
	-3.919	0.04836	-0.04834
0.2	-4.07216	0.00934	-0.00934
	-4.07215	0.01862	-0.01862
	-4.0721	0.04056	-0.04054

## 6. Conclusions

This paper was presented to study the characteristics and behaviour of unsteady stagnation-point flow and heat transfer over a permeable exponential stretching/shrinking sheet in nanofluids with slip effect, and also to find a solution which is stable and physically realizable for some parameters, namely, velocity slip, stretching/shrinking, suction, injection, and with different types of nanoparticles. The system of partial differential equations was transformed to ordinary differential equations using the similarity variables. The values of the skin friction coefficient and heat transfer coefficient were obtained by a set of initial guesses in the bvp4c program in Matlab, and were presented graphically.

The Tiwari and Das model was applied in this study and the value of the Prandtl number of water was 6.2. In order to test the stability of the first and second solutions, a stability analysis was implemented. Hence, some conclusion based on the above findings were:

1. Dual solutions were obtained when  $\varepsilon_c \leq \varepsilon$ ; no solution exists when the value of  $\varepsilon$  is less than  $\varepsilon_c$ . Besides that, dual solutions were found at any value of  $s$ , but a significant difference between the first and second solutions was apparent when  $s > 1$ , which implies that the dual solutions for the suction case were much easier to find compared to the injection case.
2. The skin friction coefficient was found to be higher for the shrinking surface than the stretching surface, and also with the presence of suction parameter compared to injection parameter. In addition, an increase in the nanoparticle volume fraction in the base fluid reduced the velocity slip between the fluid, Copper nanoparticles, and the surface, and increased the unsteadiness parameter, resulting in an increase in the skin friction coefficient.
3. The heat transfer coefficient was increased more for the stretching surface than for the shrinking surface; the same trend was observed with the existence of a suction parameter. Meanwhile, a decreasing amount of nanoparticles, an increasing value of velocity slip, the use of Copper nanoparticle, and an increase of the unsteadiness parameter also increased the heat transfer rate at the surface.
4. The velocity and the temperature of the fluid were increased when, with the stronger slip parameter, the sheet was stretched, and with the mass injection parameter.
5. The first solution was found to be stable and physically realizable, whereas the second was not stable based on the performed stability analysis.

**Author Contributions:** N.B. conceived and designed the problem; N.F.D. performed the derivation and numerical data; N.F.D., N.B. and N.A.Y. analyzed the numerical data; N.M.A. and H.R. contributed reagents/materials/analysis tools; N.F.D. wrote the paper.

**Funding:** This work is supported by Fundamental Research Grant Scheme (FRGS/1/2018/STG06/UPM/02/4), Fundamental Research Grant Scheme (FRGS/1/2017/STG06/UiTM/02/9) and the financial support received from Universiti Putra Malaysia.

**Acknowledgments:** We would like to express an appreciation to the Universiti Teknologi MARA, Universiti Putra Malaysia and Ministry of Higher Education for the scholarship and the financial support received.

**Conflicts of Interest:** The authors declare no conflict of interest.

## Nomenclature

### Roman letters

$a$	Stagnation length
$A$	dependent unsteadiness parameter
$c$	flow unsteadiness parameter
$C_f$	local skin friction
$f$	similarity function
$f_0$	function
$F, G$	functions
$l$	characteristic length
$L$	slip length
$Nu_x$	local Nusselt number
$Pr$	Prandtl number
$q_w$	heat flux at the surface
$Re_x$	local Reynold number
$s$	suction/injection parameter
$t$	time
$T$	Temperature
$T_0$	reference temperature

$T_w$	temperature at the surface
$T_\infty$	ambient temperature
$u$	velocity component in $x$ -axis
$u_w$	plate velocity
$u_s$	velocity slip
$U_\infty$	free stream velocity
$v$	velocity component in $y$ -axis
$v_0$	constant
$v_w$	mass flux velocity
<i>Greek symbols</i>	
$\alpha$	thermal diffusivity
$\mu$	viscosity
$k$	thermal conductivity
$\rho$	density
$\rho C_p$	heat capacity
$\psi$	stream function
$\varepsilon$	stretching/shrinking parameter
$\sigma$	slip parameter
$\gamma$	smallest eigenvalue
$\varphi$	nanoparticle volume fraction
$\theta$	dimensionless temperature function
$\theta_0$	function
$\tau$	dimensionless variable
$\tau_w$	shear stress at the surface
<i>Subscripts</i>	
$c$	critical value
$f$	base fluid
$nf$	nanofluid
$s$	solid nanofluid
$w$	condition at the surface
$\infty$	condition on free stream
<i>Superscript</i>	
'	differentiate with respect to $\eta$

## References

1. Yang, J.; Bos, R.; Belder, G.F.; Engel, J.; Busscher, H.J. Deposition of Oral Bacteria and Polystyrene Particles to Quartz and Dental Enamel in a Parallel Plate and Stagnation Point Flow Chamber. *J. Colloid Interface Sci.* **1999**, *418*, 410–418. [[CrossRef](#)] [[PubMed](#)]
2. Montecchio, F.; Persson, H.; Engvall, K.; Delin, J.; Lanza, R. Development of a stagnation point flow system to screen and test TiO<sub>2</sub>-based photocatalysts in air purification applications. *Chem. Eng. J.* **2016**, *306*, 734–744. [[CrossRef](#)]
3. Pavithra, G.M.; Gireesha, B.J. Unsteady flow and heat transfer of a fluid-particle suspension over an exponentially stretching sheet. *Ain Shams Eng. J.* **2014**, *5*, 613–624. [[CrossRef](#)]
4. Zaib, A.; Bhattacharyya, K.; Shafie, S. Unsteady boundary layer flow and heat transfer over an exponentially shrinking sheet with suction in a copper-water nanofluid. *J. Cent. South Univ.* **2015**, *22*, 4856–4863. [[CrossRef](#)]
5. Rao, J.A.; Vasumathi, G.; Mounica, J. Joule Heating and Thermal Radiation Effects on MHD Boundary Layer Flow of a Nanofluid over an Exponentially Stretching Sheet in a Porous Medium. *World J. Mech.* **2015**, *5*, 151–164. [[CrossRef](#)]
6. Aleng, N.L.; Bachok, N.; Arifin, N.M. Flow and Heat Transfer of a Nanofluid over an Exponentially Shrinking Sheet. *Indian J. Sci. Technol.* **2015**, *8*, 1–6. [[CrossRef](#)]
7. Bachok, N.; Ishak, A.; Pop, I. Boundary layer stagnation-point flow and heat transfer over an exponentially stretching / shrinking sheet in a nanofluid. *Int. J. Heat Mass Transf.* **2012**, *55*, 8122–8128. [[CrossRef](#)]

8. Bhattacharyya, K.; Vajravelu, K. Stagnation-point flow and heat transfer over an exponentially shrinking sheet. *Commun. Nonlinear Sci. Numer. Simul.* **2012**, *17*, 2728–2734. [[CrossRef](#)]
9. Rehman, F.U.; Nadeem, S.; Rehman, H.U.; Haq, R.U. Thermophysical analysis for three-dimensional MHD stagnation-point flow of nano-material influenced by an exponential stretching surface. *Results Phys.* **2018**, *8*, 316–323. [[CrossRef](#)]
10. Wong, S.W.; Awang, A.O.; Ishak, A. Stagnation-point flow over an exponentially shrinking/stretching sheet. *Z. Naturforsch. A* **2011**, *66*, 705–711. [[CrossRef](#)]
11. Choi, S.U.S.; Eastman, J.A. Enhancing thermal conductivity of fluids with nanoparticles. In Proceedings of the ASME International Mechanical Engineering Congress and Exposition, San Francisco, CA, USA, 12–17 November 1995; pp. 99–105.
12. Buongiorno, J. Convective transport in nanofluids. *J. Heat Transf.* **2006**, *128*, 240–250. [[CrossRef](#)]
13. Tiwari, R.K.; Das, M.K. Heat transfer augmentation in a two-sided lid-driven differentially heated square cavity utilizing nanofluids. *Int. J. Heat Mass Transf.* **2007**, *50*, 2002–2018. [[CrossRef](#)]
14. Akbari, M.; Galanis, N.; Behzadmehr, A. Comparative assessment of single and two-phase models for numerical studies of nanofluid turbulent forced convection. *Int. J. Heat Fluid Flow* **2012**, *37*, 136–146. [[CrossRef](#)]
15. Ebrahimi, A.; Rikhtegar, F.; Sabaghan, A.; Roohi, E. Heat transfer and entropy generation in a microchannel with longitudinal vortex generators using nanofluids. *Energy* **2016**, *101*, 190–201. [[CrossRef](#)]
16. Pang, C.; Jung, J.Y.; Kang, Y.T. Aggregation based model for heat conduction mechanism in nanofluids. *Int. J. Heat Mass Transf.* **2014**, *72*, 392–399. [[CrossRef](#)]
17. Firouzfard, E.; Soltanieh, M.; Noie, S.H.; Saidi, S.H. Energy saving in HVAC systems using nano fluid. *Appl. Therm. Eng.* **2011**, *31*, 1543–1545. [[CrossRef](#)]
18. Wang, E.C.; Wang, A.Z. Nanoparticles and Their Applications In Cell and Molecular Biology. *Integr. Biol.* **2014**, *6*, 9–26. [[CrossRef](#)] [[PubMed](#)]
19. Patil, M.S.; Kim, S.C.; Seo, J.; Lee, M. Review of the Thermo-Physical Properties and System Using Refrigerant-Based Nanofluids. *Energy* **2016**, *9*, 22.
20. Che Sidik, N.A.; Cheong, N.G.Y.; Fazeli, A. Computational analysis of nanofluids in vehicle radiator. *Appl. Mech. Mater.* **2015**, *695*, 539–543. [[CrossRef](#)]
21. Abu-Nada, E.; Oztop, H.F. Numerical Analysis of Al<sub>2</sub>O<sub>3</sub>/Water Nanofluids Natural Convection in a Wavy Walled Cavity. *Numer. Heat Transf. Part A Appl.* **2011**, *59*, 403–419. [[CrossRef](#)]
22. Noghrehabadi, A.; Pourrajab, R.; Ghalambaz, M. Effect of partial slip boundary condition on the flow and heat transfer of nanofluids past stretching sheet prescribed constant wall temperature. *Int. J. Therm. Sci.* **2012**, *54*, 253–261. [[CrossRef](#)]
23. Kuznetsov, A.V.; Nield, D.A. The Cheng-Minkowycz problem for natural convective boundary layer flow in a porous medium saturated by a nanofluid: A revised model. *Int. J. Heat Mass Transf.* **2013**, *65*, 682–685. [[CrossRef](#)]
24. Afshoon, Y.; Fakhar, A. Numerical Study of Improvement in Heat Transfer Coefficient of Cu-O Water Nanofluid in the Shell and Tube Heat Exchangers. *Biosci. Biotech. Res. Asia* **2014**, *11*, 739–774. [[CrossRef](#)]
25. Dinarvand, S.; Hosseini, R.; Abulhasansari, M.; Pop, I. Buongiorno's model for double-diffusive mixed convective stagnation-point flow of a nanofluid considering diffusiophoresis effect of binary base fluid. *Adv. Powder Technol.* **2015**, *26*, 1423–1434. [[CrossRef](#)]
26. Omar, N.S.; Bachok, N.; Arifin, N.M. Stagnation Point Flow Over a Stretching or Shrinking Cylinder in a Copper-Water Nanofluid. *Indian J. Sci. Technol.* **2015**, *8*, 1–7. [[CrossRef](#)]
27. Hady, F.M.; Ibrahim, F.S.; Abdel-Gaied, S.M.; Eid, M.R. Boundary-Layer Flow in a Porous Medium of a Nanofluid Past a Vertical Cone. In *An Overview of Heat Transfer Phenomena*; Kazi, S.N., Ed.; IntechOpen: London, UK, 2012; pp. 91–104.
28. Abbas, Z.; Perveen, R.; Sheikh, M.; Pop, I. Thermophoretic diffusion and nonlinear radiative heat transfer due to a contracting cylinder in a nanofluid with generalized slip condition. *Results Phys.* **2016**, *6*, 1080–1087. [[CrossRef](#)]
29. Pour, M.S.; Nassab, S.G. Numerical investigation of forced laminar convection flow of nanofluids over a backward facing step under bleeding condition. *J. Mech.* **2012**, *28*, N7–N12. [[CrossRef](#)]
30. Merkin, J.H. On dual solutions occurring in mixed convection in a porous medium. *J. Eng. Math.* **1986**, *20*, 171–179. [[CrossRef](#)]

31. Weidman, P.D.; Kubitschek, D.G.; Davis, A.M.J. The effect of transpiration on self-similar boundary layer flow over moving surfaces. *Int. J. Eng. Sci.* **2006**, *44*, 730–737. [[CrossRef](#)]
32. Harris, S.D.; Ingham, D.B.; Pop, I. Mixed convection boundary-layer flow near the stagnation point on a vertical surface in a porous medium: Brinkman model with slip. *Transp. Porous Media* **2009**, *77*, 267–285. [[CrossRef](#)]
33. Roşca, N.C.; Pop, I. Mixed convection stagnation point flow past a vertical flat plate with a second order slip: Heat flux case. *Int. J. Heat Mass Transf.* **2013**, *65*, 102–109. [[CrossRef](#)]
34. Mohd Noor, M.A.; Nazar, R.; Jafar, K. Stability analysis of stagnation-point flow past a shrinking sheet in a nanofluid. *J. Qual. Meas. Anal.* **2014**, *10*, 51–63.
35. Ishak, A. Dual solutions in mixed convection boundary layer flow: A stability analysis. *Int. J. Math. Comput. Phys. Quantum Eng.* **2014**, *8*, 1131–1134.
36. Hafidzuddin, E.; Nazar, R.; Md Arifin, N.; Pop, I. Stability Analysis of Unsteady Three-Dimensional Viscous Flow Over a Permeable Stretching/Shrinking Surface. *J. Qual. Meas. Anal.* **2015**, *11*, 19–31.
37. Najib, N.; Bachok, N.; Arifin, N. Stability of Dual Solutions in Boundary Layer Flow and Heat Transfer over an Exponentially Shrinking Cylinder. *Indian J. Sci. Technol.* **2016**, *9*, 1–6. [[CrossRef](#)]
38. Najib, N.; Bachok, N.; Arifin, N.; Senu, N. Boundary Layer Flow and Heat Transfer of Nanofluids over a Moving Plate with Partial Slip and Thermal Convective Boundary Condition: Stability Analysis. *Int. J. Mech.* **2017**, *11*, 18–24.
39. Najib, N.; Bachok, N.; Arifin, N.M.; Ali, F.M. Stability Analysis of Stagnation-Point Flow in a Nanofluid over a Stretching/Shrinking Sheet with Second-Order Slip, Soret and Dufour Effects: A Revised Model. *Appl. Sci.* **2018**, *8*, 642. [[CrossRef](#)]
40. Salleh, S.N.A.; Bachok, N.; Arifin, N.M.; Ali, F.M.; Pop, I. Stability Analysis of Mixed Convection Flow towards a Moving Thin Needle in Nanofluid. *Appl. Sci.* **2018**, *8*, 842. [[CrossRef](#)]
41. Adnan, N.S.M.; Arifin, N.M. Stability analysis of boundary layer flow and heat transfer over a permeable exponentially shrinking sheet in the presence of thermal radiation and partial slip. *J. Phys. Conf. Ser. Pap.* **2017**, *890*, 012046. [[CrossRef](#)]
42. Oztop, H.F.; Abu-Nada, E. Numerical study of natural convection in partially heated rectangular enclosures filled with nanofluids. *Int. J. Heat Fluid Flow* **2008**, *29*, 1326–1336. [[CrossRef](#)]



© 2018 by the authors. Licensee MDPI, Basel, Switzerland. This article is an open access article distributed under the terms and conditions of the Creative Commons Attribution (CC BY) license (<http://creativecommons.org/licenses/by/4.0/>).